

World Journal of *Radiology*

Monthly Volume 17 Number 10 October 28, 2025



MINIREVIEWS

Agnello F, Taibbi A, Galia M, Orlando A, Gagliardo C, Bartolotta TV. Hepatocellular carcinoma treatment response: Imaging findings and criteria. *World J Radiol* 2025; 17(10): 108804 [DOI: [10.4329/wjr.v17.i10.108804](https://doi.org/10.4329/wjr.v17.i10.108804)]

Gao QY, Wang LJ, Ma C. Diffusion-weighted magnetic resonance imaging of the pancreas: A narrative review. *World J Radiol* 2025; 17(10): 112271 [DOI: [10.4329/wjr.v17.i10.112271](https://doi.org/10.4329/wjr.v17.i10.112271)]

LETTER TO THE EDITOR

Perera Molligoda Arachchige AS. Toward rapid, practical risk stratification in spontaneous intracerebral hemorrhage. *World J Radiol* 2025; 17(10): 114449 [DOI: [10.4329/wjr.v17.i10.114449](https://doi.org/10.4329/wjr.v17.i10.114449)]

ABOUT COVER

Peer Reviewer of *World Journal of Radiology*, Abhimanyu Chand, MD, FCCM, Chief Physician, Critical Care Unit, Sushma Koirala Memorial Hospital, Shankharapur, Kathmandu 44600, Bagmati, Nepal. aabhichand@gmail.com

AIMS AND SCOPE

The primary aim of *World Journal of Radiology (WJR, World J Radiol)* is to provide scholars and readers from various fields of radiology with a platform to publish high-quality basic and clinical research articles and communicate their research findings online.

WJR mainly publishes articles reporting research results and findings obtained in the field of radiology and covering a wide range of topics including state of the art information on cardiopulmonary imaging, gastrointestinal imaging, genitourinary imaging, musculoskeletal imaging, neuroradiology/head and neck imaging, nuclear medicine and molecular imaging, pediatric imaging, vascular and interventional radiology, and women's imaging.

INDEXING/ABSTRACTING

The *WJR* is now abstracted and indexed in PubMed, PubMed Central, Emerging Sources Citation Index (Web of Science), Reference Citation Analysis, China Science and Technology Journal Database, and Superstar Journals Database. The 2025 Edition of Journal Citation Reports® cites the 2024 journal impact factor (JIF) for *WJR* as 1.5; JIF without journal self cites: 1.4; 5-year JIF: 1.6; JIF Rank: 137/212 in radiology, nuclear medicine and medical imaging; JIF Quartile: Q3; and 5-year JIF Quartile: Q3.

RESPONSIBLE EDITORS FOR THIS ISSUE

Production Editor: *Yue-Yuan Lei*; Production Department Director: *Si Zhao*; Cover Editor: *Jia-Ping Yan*.

NAME OF JOURNAL

World Journal of Radiology

ISSN

ISSN 1949-8470 (online)

LAUNCH DATE

January 31, 2009

FREQUENCY

Monthly

EDITORS-IN-CHIEF

Thomas J Vogl

EDITORIAL BOARD MEMBERS

<https://www.wjgnet.com/1949-8470/editorialboard.htm>

PUBLICATION DATE

October 28, 2025

COPYRIGHT

© 2025 Baishideng Publishing Group Inc

INSTRUCTIONS TO AUTHORS

<https://www.wjgnet.com/bpg/gerinfo/204>

GUIDELINES FOR ETHICS DOCUMENTS

<https://www.wjgnet.com/bpg/GerInfo/287>

GUIDELINES FOR NON-NATIVE SPEAKERS OF ENGLISH

<https://www.wjgnet.com/bpg/gerinfo/240>

PUBLICATION ETHICS

<https://www.wjgnet.com/bpg/GerInfo/288>

PUBLICATION MISCONDUCT

<https://www.wjgnet.com/bpg/gerinfo/208>

ARTICLE PROCESSING CHARGE

<https://www.wjgnet.com/bpg/gerinfo/242>

STEPS FOR SUBMITTING MANUSCRIPTS

<https://www.wjgnet.com/bpg/GerInfo/239>

ONLINE SUBMISSION

<https://www.f6publishing.com>

Diffusion-weighted magnetic resonance imaging of the pancreas: A narrative review

Qing-Yu Gao, Li-Jia Wang, Chao Ma

Specialty type: Radiology, nuclear medicine and medical imaging

Provenance and peer review: Unsolicited article; Externally peer reviewed.

Peer-review model: Single blind

Peer-review report's classification

Scientific Quality: Grade A, Grade B, Grade B, Grade C

Novelty: Grade A, Grade A, Grade B, Grade C

Creativity or Innovation: Grade A, Grade B, Grade B, Grade C

Scientific Significance: Grade A, Grade B, Grade B, Grade C

P-Reviewer: Niu L, Additional Professor, China; Pappachan JM, MD, FRCP, MRCP, Professor, Senior Researcher, United Kingdom; Ravi PK, MD, Assistant Professor, India

Received: July 22, 2025

Revised: August 20, 2025

Accepted: October 10, 2025

Published online: October 28, 2025

Processing time: 98 Days and 2.9 Hours



Qing-Yu Gao, Li-Jia Wang, School of Health Science and Engineering, University of Shanghai for Science and Technology, Shanghai 200093, China

Qing-Yu Gao, Chao Ma, Department of Radiology, Changhai Hospital of Shanghai, Naval Medical University, Shanghai 200433, China

Chao Ma, College of Electronic and Information Engineering, Tongji University, Shanghai 201804, China

Corresponding author: Chao Ma, MS, Professor, Department of Radiology, Changhai Hospital of Shanghai, Naval Medical University, No. 168 Changhai Road, Shanghai 200433, China. machaohdsd@126.com

Abstract

Diffusion-weighted magnetic resonance imaging (DWI) has become an essential tool in the field of pancreatic magnetic resonance imaging, enabling the detection, characterization, prediction, and evaluation of pancreatic diseases. In this article, we review the acquisition parameters, postprocessing techniques, and quantitative methods utilized in pancreatic DWI. Various postprocessing models, including monoexponential, biexponential, stretched exponential and non-Gaussian kurtosis models, as well as deep learning networks, have been used to assess the clinical utility of these models in diagnosing pancreatic diseases. The single-shot echo-planar imaging sequence is the most commonly used sequence for DWI data acquisition in clinical settings, and the apparent diffusion coefficient (ADC) calculated using the monoexponential model is the most widely used quantitative parameter in clinical practice. The repeatability threshold for the ADC of a normal pancreas is 37% for test-retest scans, but the repeatability threshold for pancreatic tumors needs to be further investigated. Complex postprocessing models exploring novel DWI-based biomarkers beyond ADC to assess histological features, and artificial intelligence in DWI postprocessing and data analyses hold promise in the diagnosis of pancreatic diseases. Future work should focus on standardizing protocols, conducting multicentre studies, and exploring variety of methods to improve the accuracy of quantitative DWI results to increase the clinical effectiveness of DWI in patients with pancreatic diseases.

Key Words: Diffusion-weighted imaging; Pancreas; Magnetic resonance imaging; Model; Artificial intelligence

Core Tip: The development of diffusion-weighted magnetic resonance imaging (DWI) has been important for advancing pancreatic magnetic resonance imaging. In this article, we offer a narrative review of the utilization of both foundational DWI techniques and deep learning algorithms in the diagnosis of pancreatic disorders. Additionally, we delve into the possible advantages of employing sophisticated models in DWI data analysis for the detection and diagnosis of pancreatic diseases.

Citation: Gao QY, Wang LJ, Ma C. Diffusion-weighted magnetic resonance imaging of the pancreas: A narrative review. *World J Radiol* 2025; 17(10): 112271

URL: <https://www.wjgnet.com/1949-8470/full/v17/i10/112271.htm>

DOI: <https://dx.doi.org/10.4329/wjr.v17.i10.112271>

INTRODUCTION

Diffusion-weighted magnetic resonance imaging (DWI) is a quantitative magnetic resonance imaging (MRI) technique that uses gradient pulses to detect and measure the diffusion of water molecules in tissues, which is quantified as the apparent diffusion coefficient (ADC). DWI is applicable across various organs, in both tumor and nontumor environments, to qualitatively and quantitatively assess various pathological conditions[1]. Currently, the single-shot echo-planar imaging (SS-EPI) sequence is among the most commonly used DWI acquisition techniques in clinical practice; it offers a rapid acquisition speed, thus reducing motion artefacts and scanning time, but it is prone to magnetic susceptibility artefacts, leading to limited image spatial resolution. Readout-segmented EPI (Rs-EPI) DWI[2] and reduced field-of-view (rFOV) DWI[3,4], have improved spatial resolution in pancreatic DWI.

Initially, owing to the presence of artefacts and pitfalls, DWI was primarily focused on neuroimaging[5]. To date, advancements in hardware and software have enabled the extensive study of DWI in various clinical scenarios throughout the body, including identifying benign and malignant lesions, distinguishing different types of malignant tumors, and evaluating treatment response[6,7]. The Quantitative Imaging Biomarker Alliance (QIBA) has been striving to standardize quantitative imaging biomarkers for both clinical trials and practice[8] and has provided valuable insights into the acceptable levels of variance for the ADC. This knowledge is crucial for fully leveraging the ADC as a quantitative imaging metric for lesions in the head (8%), liver (27%), breast (27%), and prostate (15%)[9]. However, DWI has certain limitations in pancreatic imaging. Challenges in obtaining high-quality DWI arise from factors such as motion artefacts caused by respiration, peristalsis, and blood flow. Therefore, recognizing and addressing these limitations in pancreatic applications is essential to ensure that DWI can play an optimal role in the diagnosis and assessment of pancreatic diseases. Additionally, artificial intelligence plays an important role in DWI data analysis, increasing the accuracy and efficiency of quantitative assessments.

In this study, we review the acquisition technology of DWI and the application of commonly used postprocessing models in the pancreas and introduce some complex models and deep learning in DWI postprocessing to highlight their potential applications in pancreatic diseases. In conducting this review, we primarily adopted a narrative approach, while also incorporating quantitative data from previous studies. This information pertained to the application of DWI in the pancreas, including specific scanning settings and its role in the diagnosis of pancreatic diseases.

BASIC PRINCIPLES OF DWI

DWI sequences

SS-EPI is widely recognized as the preferred method for integrating DWI with fat-suppression techniques[10]. To minimize the influence of motion artefacts, both breath-hold and free-breathing technologies are utilized alongside diverse signal acquisition strategies, which may include respiratory and/or cardiac triggering. Free-breathing sequences, in particular, provide a superior signal-to-noise ratio (SNR) and accommodate a broader range of b values than the breath-hold sequences do.

Rs-EPI, a powerful imaging technique, is a multishot sequence that has been utilized in some anatomical regions, including the brain[11], breasts[12,13], prostate[14], kidneys[15] and joints[16]. Rs-EPI significantly mitigates susceptibility artefacts and T2 decay-induced blurring, thereby enhancing the quality of DWI images and the reliability of quantitative parameters. However, the prolonged acquisition time may limit its clinical utility. Advancements in imaging technology have led to the development of rFOV-DWI as an innovative solution. This technique offers improved image quality, superior tissue resolution, and a substantial reduction in artefacts and distortion[4,17]. Therefore, this method presents a promising solution for addressing the constraints associated with conventional full-FOV DWI. rFOV-DWI leverages 2D RF along with 180° pulse-back technology to minimize the signal loss resulting from the uneven B1 field distribution in the pancreatic region[17]. This approach effectively overcomes resolution challenges while increasing the

quality of pancreatic images. In contrast to the multishot techniques aimed at improving DWI clarity and reducing image distortion, rFOV-DWI avoids complex reconstruction processes[18,19]. However, its limitation lies in the small field-of-view (FOV), which may hinder the evaluation of areas beyond the imaging FOV, such as the peripancreatic lymph node status.

Parameters for DWI

In DWI, an important parameter known as the b value, also known as the diffusion factor, represents the sensitivity of the sequence to diffusion motion and serves as an indicator for detecting the ability to capture diffusion motion. The b value

is defined as follows: $b = \gamma^2 G^2 \delta^2 \left(\Delta - \frac{\delta}{3} \right)$ (1). Where G represents the magnitude of the diffusion gradient, δ denotes the duration for which the gradient is applied, and Δ signifies the time interval between two diffusion gradients. Given the physical constraints on the maximum achievable diffusion gradient, the value of G is subject to an upper limit. Consequently, when G reaches its maximum, the b value can be increased only by adjusting either δ or Δ .

The magnitude of the b value of DWI significantly affects image quality and lesion detection. Therefore, the selection of appropriate b values tailored to specific anatomical regions is crucial for accurate lesion evaluation. In abdominal DWI, the commonly utilized ranges for low and high b values are typically between 0 and 100 s/mm² and between 500 and 1500 s/mm², respectively. DWI with high b values tends to reflect restricted diffusion and thus increases the detectability of lesions in images. Koc *et al*[20] reported that a high b value of 600 s/mm² on 1.5-T MRI was optimal for distinguishing between benign and malignant lesions in the abdomen. Specifically for the pancreas, Fukukura *et al*[21] demonstrated that increasing the b value from 500 s/mm² to 1500 s/mm² on 3.0-T MRI can improve the visibility of pancreatic adenocarcinoma. This improvement is attributed to the reduction in the signal from the distal pancreas, whereas the signal from pancreatic adenocarcinoma remains significantly elevated. However, increasing the b value beyond 2000 s/mm² can decrease the image quality. This decrease is attributed to the fact that while higher b values can augment contrast, they also reduce the SNR and increase the susceptibility to artefacts.

DWI models

Numerous models are available for the quantitative assessment of the pancreas *via* DWI, including the monoexponential model, intravoxel incoherent motion (IVIM), stretched exponential model (SEM), diffusion kurtosis imaging (DKI) model, and many others. The most commonly used models for quantitative assessment involve calculating the ADC *via* a monoexponential model and estimating the derived parameters from the IVIM, which is based on biexponential analyses [22]. The fitting equations for these two models are as follows: Monoexponential model:

$$S = S_0 \exp(-b \cdot \text{ADC}) \quad (2).$$

$$\text{IVIM: } S = S_0 (f \exp(-b \cdot D^*) + (1 - f) \exp(-b \cdot D)) \quad (3).$$

In the IVIM model, three main parameters are quantified. D^* represents the perfusion information, also known as the perfusion coefficient, which mainly represents the contribution of perfusion to the attenuation of the diffusion image signal. D reflects the true diffusion information, also known as the actual diffusion coefficient, which mainly represents the contribution of true diffusion to the attenuation of the diffusion image signal, and f is the perfusion fraction, reflecting the proportion of perfusion.

SEM, proposed by Bennett *et al*[23], is a model that can simultaneously quantify water molecule diffusion capability and voxel heterogeneity[24]. Compared with the traditional exponential decay model, SEM can better describe complex diffusion processes and tissue heterogeneity. The equation for the SEM is shown in formula (4):

$$S = S_0 \exp(-(b * \text{DDC})^\alpha) \quad (4). \quad S(b) = S_0 \exp\left(-b * D + \frac{b^2 D^2 K}{6}\right) \quad (5).$$

The DKI model can be used to quantify the degree of deviation from the Gaussian distribution[25]. Formula (5) can be used to obtain the diffusion kurtosis coefficient (K). K represents the deviation of the diffusion behaviour from the Gaussian model and the degree of tissue structure confinement and heterogeneity in the tissue composition. The diffusion coefficient (D) is used to correct for non-Gaussian bias.

These models have been proposed for exploring the microstructural characteristics of tissues and investigating disease diagnosis and efficacy evaluation. Furthermore, with the rapid progression of deep learning technologies, the incorporation of deep neural networks (DNNs) into these foundational models improves the precision of quantitative parameter estimation. As a result, we can more comprehensively understand the pancreatic microenvironment and design more efficacious strategies for disease diagnosis and treatment by leveraging deep learning techniques to analyze DWI data.

APPLICATION OF DWI IN PANCREATIC DISEASES

DWI contrast is related to tissue cellularity, tissue structure, and cell membrane integrity. The use of the ADC map in differentiating and diagnosing various pancreatic diseases has been reported. Abuzeid *et al*[26] measured the average pancreatic ADC values in a small sample of acute pancreatitis patients and healthy controls. They reported that the optimal ADC threshold for distinguishing between the two groups was 1.32×10^{-3} mm²/s, with a sensitivity of 81.25%, a specificity of 93.75%, and an accuracy of 91.8%. Several studies evaluating chronic pancreatitis (CP) have reported that the ADC values in patients with CP are lower than those in healthy controls[27,28]. Therefore, DWI can serve as an adjunctive tool for diagnosing pancreatitis. Zhu *et al*[29] reported an ADC sensitivity of 83% in differentiating benign and malignant lesions, with a specificity of 87% and an area under the curve (AUC) of 0.92. Several studies have focused on

the use of DWI to discriminate between autoimmune pancreatitis (AIP) and pancreatic ductal adenocarcinoma (PDAC). Given the overlapping clinical and radiological characteristics of mass-forming pancreatitis and PDAC, differentiating them is difficult. Nevertheless, a correct diagnosis is important because the treatment and prognosis of these two diseases significantly differ[30]. Several studies[31-35] have reported ADC cut-off values ranging from 0.88 to $1.26 \times 10^{-3} \text{ mm}^2/\text{s}$ for differentiating between mass-forming pancreatitis and PDAC. However, Ha *et al*[36] reported that the ADC was ineffective in differentiating PDAC from mass-forming pancreatitis, and a comparison of ADCs for mass-forming pancreatitis and PDAC in different studies led to conflicting conclusions. Therefore, more advanced models may be needed to further investigate. In a study by De Robertis *et al*[37], the perfusion fraction (*f*) led to 100% sensitivity in distinguishing PDAC tissue from normal pancreas tissue and AIP tissue from normal pancreatic tissue. Zeng *et al*[38] measured IVIM parameters, correlated them with histopathological data, and achieved superior performance in differentiating nonhypervascular pancreatic neuroendocrine tumors (PNETs) and PDAC. Notably, *D* was found to be more effective than both the ADC and the perfusion fraction *f*. Additionally, the ADC has been consistently shown to be significantly correlated with tissue-determined pancreatic fibrosis[39-41]. DWI and corresponding ADC maps of the normal pancreas and nine representative pancreatic pathologies are shown in Figure 1.

DWI can be used to differentiate between benign and malignant tissues, and numerous studies have demonstrated that the ADC and *f* measurements are the most precise parameters. IVIM employs a biexponential model to quantify the macroscopic diffusion of water and the microscopic perfusion of blood in capillaries. IVIM-DWI can provide more refined tissue characterization and improve the discrimination between benign and malignant tissues[42]. Significant progress has been made in the use of IVIM parameters in the early detection of CP[43], the prediction of the pathological grade of pancreatic cancer, the determination of lymph node metastasis, and the differentiation of various pancreatic diseases. Liu *et al*[44] explored the correlation between IVIM parameters and pancreatic fibrosis. Their findings indicated that the *D* and *f* values increased the sensitivity and diagnostic performance for grading PDAC. McCullum *et al*[45] employed histogram analysis of the median, standard deviation, skewness, kurtosis, and percentile to compare the parameter distributions of patients with pancreatic cancer before and after treatment response by using IVIM-WI. They reported that *f* and *D* changed substantially, whereas *D** showed no significant correlation in any test. These results imply that the *f* and *D* parameters may be potential indicators for evaluating the treatment response of patients with pancreatic cancer. However, Zhu *et al*[29] systematically evaluated the ability of IVIM to distinguish between benign and malignant pancreatic lesions. They reported that IVIM exhibited high sensitivity and specificity (84% and 83%, respectively). The performance in terms of these values was comparable to the performance of the ADC values (83% and 87%, respectively). Multi-*b*-value IVIM also has challenges because of its high parameter variability and reproducibility, as well as its complexity and long acquisition times. Consequently, although the biexponential IVIM model has been extensively investigated, its routine application in diagnosing pancreatic diseases has not yet been established, and consensus on the selection of appropriate *b* values is lacking.

Research on the application of SEM in pancreatic DWI is limited. Currently, SEM is primarily used to differentiate between different types of pancreatic tumors. Shi *et al*[46] compared the correlations between different parameters *via* various methods and reported that α has significant potential in distinguishing PDAC from PNET, thus improving the diagnostic accuracy. Li *et al*[47] conducted a volume histogram analysis for each DWI parameter and compared the histogram indices obtained from different tumor parameters. They reported that volume histogram analysis of the SEM could be used to differentiate PDAC from PNET. However, the median *f* value obtained from IVIM DWI was more valuable than the ADC, *D_p*, *DDC*, and α values were. Therefore, SEM, with its ability to elucidate the intricate tissue characteristics and biological behaviour of pancreatic tumors, holds promise for refining early diagnostic procedures and optimizing therapeutic outcomes.

DKI was initially developed for neuroimaging research, which focused primarily on capturing microstructural information related to diffusion in the grey and white matter of the brain[48]. This technique examines the degree of diffusion restriction in tissue structures and the components of intra- and extracellular diffusion[49]. The typical *b*-value range for DKI is between 0 and $3000 \text{ mm}^2/\text{s}$, with high *b*-values often falling within the range of $2000\text{-}3000 \text{ mm}^2/\text{s}$ [50]. As the application of DKI models continues to expand, their use for tumor characterization and grading has garnered significant interest. Tumor tissue is distinct from normal neural tissue, leading to variations in scanning protocols and significantly reduced acquisition times. Unlike neural tissues, which exhibit strong anisotropy and require multiple scanning directions or diffusion kurtosis tensor calculations, tumor tissues generally do not require such approaches. In many cases, the mean diffusion (*MD*) and mean kurtosis (*MK*) of tissues can be obtained in much shorter scanning times. DKI has been widely applied to various abdominal organs, including the prostate[51], kidney[52], and cervix[53], demonstrating greater clinical value than traditional DWI techniques do. In the field of pancreatic imaging, a study conducted by Granata *et al*[54] revealed that the *MD* can be used to effectively differentiate between pancreatic parenchyma, peritumoral inflammation, and pancreatic tumors. Furthermore, Mayer *et al*[55] suggested that the DKI-derived parameter *D* can serve as a noninvasive biomarker for evaluating the composition of stromal tissue in PDAC. In terms of treatment response evaluation, Granata *et al*[56] reported significant changes in the *MD* parameter obtained from DKI before and after electrochemotherapy in pancreatic cancer patients, and excellent diagnostic performance was achieved (sensitivity = 0.8, specificity = 1.0, AUC = 0.933). Zhang *et al*[57] assessed the efficacy of first-line chemotherapy in unresectable pancreatic cancer patients *via* DKI and reported that the *MD* (sensitivity = 85.7%, specificity = 85.7%, AUC = 0.898) outperformed the ADC in terms of diagnostic performance. These findings highlight the potential of DKI in characterizing pancreatic lesions, assessing treatment response, and improving diagnostic accuracy.

The variability of quantitative parameters is important when considering the application of DWI quantitative parameters. In accordance with the recommendations of the QIBA, the ADC variation threshold can be calculated using the following formula[8,9]: Scaled percent repeatability coefficient = $2.77 \times$ weighted coefficient of variation (*wCV*) \times 100%.

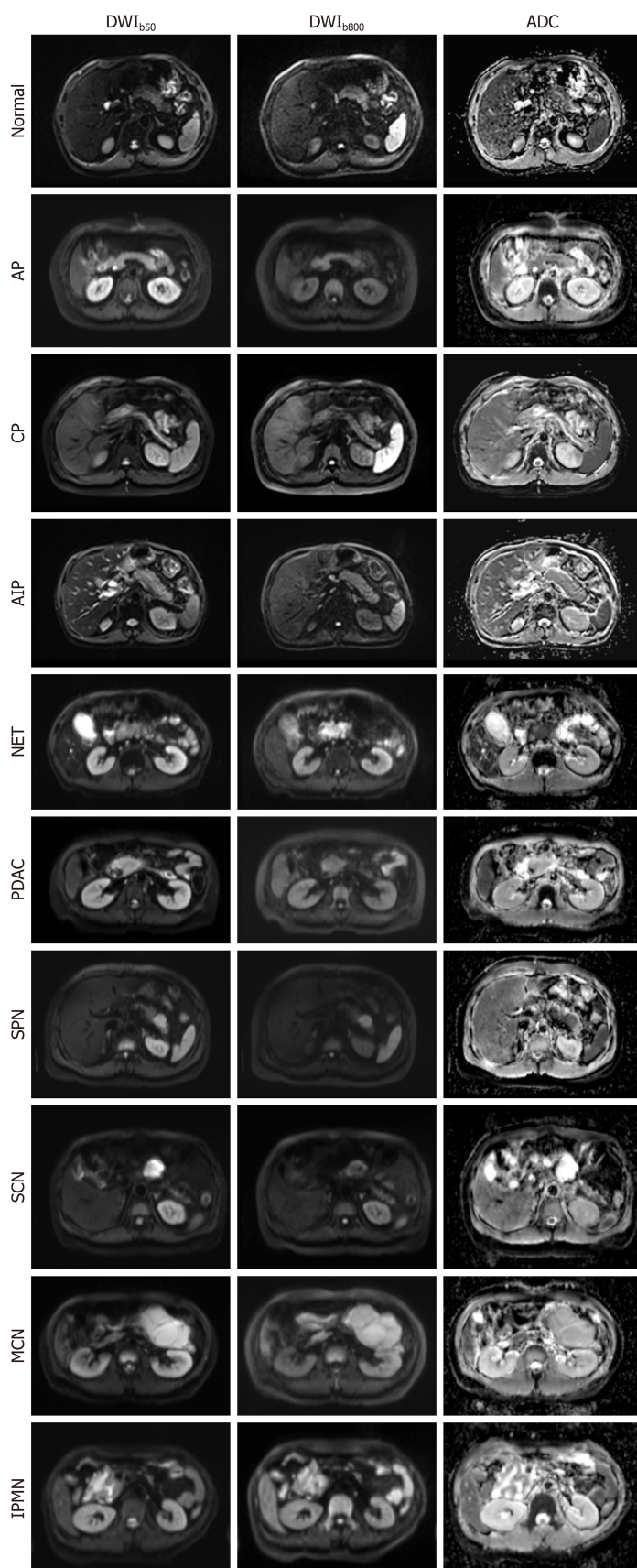


Figure 1 Diffusion-weighted imaging and corresponding apparent diffusion coefficient maps of the normal pancreas and nine representative pancreatic pathologies, acquired on a 3.0-T system with b-values of 50 and 800 s/mm². AP: Acute pancreatitis; CP: Chronic pancreatitis; AIP: Autoimmune pancreatitis; NET: Neuroendocrine tumor; PDAC: Pancreatic ductal adenocarcinoma; SPN: Solid-pseudopapillary neoplasm; SCN: Serous cystic neoplasm; MCN: Mucinous cystic neoplasms; IPMN: Intraductal papillary mucinous neoplasm; DWI: Diffusion-weighted magnetic resonance imaging; ADC: Apparent diffusion coefficient.

The wCV can be derived from previous studies, and computed using the reported sample size for each study as a weighted factor.

$$wCV = \sqrt{(\sum_{i=1}^n wCV_i^2 \times N_i) / (\sum_{i=1}^n N_i)} \quad (6)$$

Here, wCV_i represents the wCV from the *i*th article out of a total of *n* articles, and *N_i* denotes the sample size from the *i*th study. According to previous findings[58-60], the repeatability threshold for the ADC of the normal pancreas is 37% (38%, 35% and 37% for the head, neck and tail of the pancreas, respectively) for test-retest scans. However, relevant research data for pancreatic tumors are scarce. Therefore, determining the repeatability threshold for the ADC of pancreatic tumors and other quantitative parameters requires further investigation.

DEEP LEARNING IN DWI DATA ANALYSES

The emergence of deep learning has led to significant advancements in the field of medical imaging. Researchers have successfully applied DNNs to fit IVIM, as exemplified by the work of Barbieri *et al*[61]. By employing unsupervised learning training with DNNs, they generated more detailed parameter maps, reduced noise levels, and accelerated generation speeds compared with conventional methods, such as the least squares trust region algorithm and Bayesian probability-based IVIM fitting. Another noteworthy development by Kaandorp *et al*[62] involved the utilization of unsupervised physics-informed DNNs (PI-DNNs) for IVIM modelling. By incorporating the consistency between IVIM predictions and measured signals as a loss term in DNNs, they were able to train the unsupervised PI-DNN directly on patient data without the need for ground truth. This approach resulted in the successful development and training of IVIM-NET, a method that can accurately and independently predict IVIM parameters in patients with PDAC[63,64]. Building upon this groundwork, Troelstra *et al*[65] developed an unsupervised PI-DNN known as IVIM-NET, which is based on a triple-exponential IVIM. They evaluated the performance of this model in the context of nonalcoholic fatty liver disease and revealed a strong correlation with histopathology. The performance of this model surpassed that of traditional least-squares methods. Shi *et al*[66] combined diffusion-weighted (DW) images with convolutional neural networks (CNNs) to transform multi-b-value DW images into histogram arrays, which were subsequently employed as inputs for a 2D CNN model. This approach enables the differentiation of various pancreatic tumor types, including PDAC, PNET, and solid pseudopapillary neoplasm. These studies collectively highlight the profound benefits of integrating deep learning networks into DWI modelling, facilitating more precise and efficient analysis of medical images while improving our understanding and diagnostic capabilities across a range of diseases.

DIFFUSION-RELAXATION DWI

Although basic DWI models have been widely used in the clinical monitoring of diseases, they provide limited micro-structural information[67,68]. To improve disease diagnosis, researchers have employed hybrid multidimensional MRI techniques to acquire specific parameter maps, which are feasible in terms of imaging time and image quality for the clinical application of abdominal organs. Furthermore, the maps derived from hybrid multidimensional MRI could be used to quantify the histological compartments of tumors. In several studies on prostate and other abdominal organ cancers[69-73], the combination of T2-weighted imaging with DWI data has been shown to increase diagnostic accuracy [74,75]. This method has demonstrated an overall sensitivity of 76% and a specificity of 82% in prostate cancer detection [76]. Zhang *et al*[72] utilized *ex vivo* diffusion relaxation correlation spectroscopic imaging (DR-CSI)[77] to quantify T2 relaxation and diffusion (T2-D) component spectra, which constitute the entire MRI signal in each voxel. By integrating the T2-D spectral peaks on a voxel basis, they generated signalling component fraction maps, characterizing the application value of DR-CSI in the compartmental quantification of *ex vivo* prostate specimens from prostate cancer patients. DR-CSI employs an improved two-dimensional ss-EPI sequence, simulating the sum of continuous exponential decay functions for each MRI signal voxel by acquiring multiple echo times and corresponding b values. This process enables the characterization of T2 and D as follows:

$$S(x, y, TE, b) = \omega(x, y, T2, D) \iint \exp\left(-\frac{TE}{T2}\right) \exp(-b * D) dT2dD = L\omega \quad (7)$$

Where *S* (*x*, *y*, *TE*, *b*) represents the measured signal in the voxel for each TE-*b* data point, while ω (*x*, *y*, *T2*, *D*) represents the T2-D spectrum to be reconstructed for the voxel. The Laplace transform is denoted by *L*. To solve for ω (*x*, *y*, *T2*, *D*), a nonnegativity constraint and a regularization term are applied.

$$\omega = \operatorname{argmin} \|S - L\omega\|_2^2 + \alpha \|\omega\|_2^2, \omega \geq 0 \quad (8)$$

Each peak in the T2-D spectrum represents a separate signalling component, allowing for the calculation of signalling component fractions in voxels or spatial regions.

$$f_A(x, y) = \frac{\iint_{\text{Area under peak A}} \omega(x, y, T2, D) dT2dD}{\iint_{\text{entire}(T2-D)\text{space}} \omega(x, y, T2, D) dT2dD} \quad (9)$$

Currently, this technique has been extensively studied for organs such as the kidney[78], liver[79], and cervix[80]. In clinic, multi-TE and multi-b value data associated with each voxel can be obtained. The following equation is subsequently used to calculate the tissue composition volumes in each voxel.

$$\frac{S(x_i, y_i, b_p, TE_p)}{S_0(x_i, y_i, b_p, TE_p)} = \sum_{i=1}^N \omega_i f(x_i, y_i, T_2^q, D_q) \exp\left(-\frac{TE_p}{T_2^q}\right) \exp\left(-b^p * ADC^q\right) \quad (10)$$

Where $i = 1, \dots, N$ and represents the position of the i^{th} voxel. P indicates the number of combinations of b , and TE ω denotes the density normalization factor associated with the Riemann sum. S represents the signal intensity corresponding to different combinations of TE s and b values, whereas S_0 represents the signal intensity at the lowest echo time and b value. The quantitative T_2 and ADC values are obtained by fitting a single exponential decay model. The function represents the two-dimensional diffusion-relaxation correlation spectrum, which provides the volume fraction of different tissue components in each voxel. Chatterjee *et al*[73] reported a strong correlation between tissue composition measured *via* hybrid multidimensional MRI and quantitative histological evaluations. The results for prostate tissue components (stroma, epithelium, and lumen) obtained *via* these methods are highly consistent with the pathological results. To date, the application of these complex models to calculate tissue quantification maps and analyze tumor tissue characteristics has been preliminarily explored under conditions such as pituitary adenomas[81] and parotid gland tumors[82]. Nevertheless, research in a specific domain of pancreatic tumors has not yet been conducted. Consequently, considering the pronounced lumen structure of pancreatic tissue, this advanced imaging technique can be applied to pancreatic tumors in a murine model. This application warrants a thorough feasibility analysis and could provide novel insights into the intricate microarchitecture and pathological profiles of the abovementioned tumors.

Optimizing post-processing parameters for tumor DWI remains a challenging task, and rigorous validation against histopathology is indispensable for clinical translation. To accelerate the clinical application of diffusion techniques, the development of an open-source tool, community-driven platform is imperative. Such a shared resource would offer researchers and clinicians a standardized framework to implement and optimize DWI postprocessing models, thereby increasing the accuracy of tumor characterization and guiding personalized therapy.

DISCUSSION

Currently, 1.5 Tesla (1.5-T) and 3 Tesla (3.0-T) MRI systems are commonly used in the clinic for examinations across various anatomical regions of patients. A systematic review revealed that the superiority of 3.0-T over 1.5-T for pancreatic DWI has not been proven, because of a lack of published studies[83]. However, in recent years, the clinical application of 3.0-T MRI for pancreatic detection has significantly increased, with the number of studies conducted at 3.0-T being comparable to those at 1.5-T. Therefore, DWI using 3.0-T units clearly enhances the diagnostic performance for pancreatic lesions[29] because of the advantages offered by the 3.0-T system, such as improved SNR[82,84,85]. Previous studies have already advocated the use of DWI for both the detection and characterization of pancreatic disorders[86-88]. With the maturation of ultrahigh-field technology, feasibility has been established for 5.0-T, 7.0-T, and even 11.7-T MRI. Rosenkrantz *et al*[89] reported that the subjective image quality of abdominal DWI at 3.0-T is significantly inferior to that at 1.5-T. However, several studies have demonstrated that when combined with the rFOV-DWI technique, 5.0-T MRI can improve the quality of pancreatic images[82-84]. Zheng *et al*[90] and Zhang *et al*[91] compared the subjective image quality ratings of DW images acquired *via* the rFOV-DWI technique with those of 3.0-T MRI and 5.0-T MRI, and confirmed that the subjective image quality at 5.0-T was significantly greater than that at 3.0-T. Jiang *et al*[92] measured ADC values in normal pancreatic tissue and reported high stability, repeatability, and consistency, indicating that 5.0-T DWI can be a reliable tool for clinical pancreatic diagnosis and that rFOV-DWI is a feasible quantitative imaging tool for studying pancreatic lesions. Moreover, 7.0-T MRI is currently a limited choice for high-field MRI in human imaging and is applicable only to the head[93-95] and limbs[96]. The use of ultrahigh-field MRI is limited to preclinical animal experiments. Fujiwara *et al*[97] evaluated the correlation between IVIM parameters and ischaemic changes in the rat cerebral cortex *via* a preclinical ultrahigh-field 11.7-T MRI scanner. In a study by Zhang *et al*[98], conventional DWI, IVIM, and DKI were performed to assess pancreatic fibrosis in a rat model of CP. They validated the effectiveness of diffusion parameters such as the ADC , D , MD , and MK in evaluating the staging of pancreatic fibrosis. In summary, 1.5-T and 3.0-T imaging remain the mainstream choices. In this context, the stability of parameter measurements and the impact of postprocessing algorithms on the results are crucial factors that different research teams are continuously striving to address. Therefore, we recommend the development of an open-source mathematical framework and the open exchange of domain expertise. Such collaborative initiatives will increase the accuracy and reliability of DWI, ultimately accelerating progress in the diagnosis and treatment of pancreatic disease.

The postprocessing of DWI data must be considered to translate research findings into clinical practice. However, the feasibility of applying complex models from the brain to the abdomen remains uncertain. Consequently, obtaining high-quality images, which should not only have high resolution but also minimize negative factors that affect image quality, such as motion artefacts, cardiac pulsation, and gastrointestinal peristalsis, are valuable for conducting clinical validation experiments, designing suitable animal models, and utilizing dedicated imaging instruments. Additionally, animal models can provide detailed pathological information, which is valuable for revealing the potential characteristics of tumors and changes after treatment. Furthermore, certain research groups in the field of prostate studies have provided superior samples, which can serve as valuable references[63-65].

THE CURRENT CHALLENGES AND FUTURE DEVELOPMENT TRENDS

The current challenges in using DWI to diagnose pancreatic disease are twofold: Image quality and imaging time. The pancreas is particularly prone to artefacts because of its small size and proximity to the gas- and air-filled structures of the upper gastrointestinal tract. These structures cause motion and susceptibility artefacts, which can degrade image quality and complicate the radiological decision-making process, especially in exams with a high artefact burden. The high

susceptibility to artefacts in abdominal DWI may stem from motion caused by gastric and bowel movement, as well as respiratory motion. This motion can hinder the discernment of small lesions, which are potentially highly relevant for diagnosis. Increasing spatial resolution to balance imaging time and image quality, including SNR and spatial resolution, can lead to a rapid decrease in the SNR of DWI. This decrease may result in a noise floor bias in the measurements of quantitative parameters, which in turn limits the application of DWI in pancreatic imaging. Therefore, MRI equipment manufacturers, research teams, and clinicians are continuously better MRI hardware facilities, such as more powerful gradients, and advanced imaging methods, including the use of artificial intelligence, to achieve rapid and high-quality pancreatic DWI.

Quantitative DWI parameters, including ADC values, may be subject to variations due to biological factors, technical factors, and measurement errors. Establishing reference standards for DWI and quantitative analysis, and promoting them on a global scale, as suggested by organizations such as the QIBA, is of paramount importance. Additionally, multi-centre trials are urgently needed to enhance the applications of DWI in pancreatic diseases is one of the urgently needed tasks.

The clinical application of newly developed high-field MRI systems, such as 5.0-T, has yet to be fully evaluated in pancreas diagnostics, particularly regarding the quality, stability, and repeatability of DWI. Current reports are limited by small cohorts and an almost exclusive focus on healthy volunteers, leaving the generalizability to pancreatic pathology unknown. These challenges underscore the need for further advancements in DWI and techniques to improve image quality, reduce artefacts, and enhance the diagnostic accuracy of pancreatic disease diagnosis.

CONCLUSION

DWI is currently the most widely utilized quantitative sequence in pancreatic imaging and has good contrast for visualizing tumors, as it easily captures abnormal tumor regions. However, despite its extensive application in pancreatic imaging, the potential of various quantitative parameters of various DWI models in the pancreas remains largely unexplored. This presents an opportunity for further research and exploration to reveal the potential value of these quantitative parameters in the diagnosis and treatment of pancreatic diseases. Through continued investigation and innovation in image data acquisition, reconstruction, quantitative parameter map generation, quality assurance and interpretation, we anticipate more breakthroughs in pancreatic imaging that will offer increased diagnostic accuracy and reliable treatment strategies for clinical practice.

FOOTNOTES

Author contributions: Gao QY wrote the paper; Wang LJ and Ma C performed the collected the data. All authors reviewed and edited the paper.

Supported by National Natural Science Foundation of China, No. 62472315; and Shanghai Science and Technology Innovation Action Plan Medical Innovation Research Project, No. 20Y11912500.

Conflict-of-interest statement: Authors declare no conflict of interests for this article.

Open Access: This article is an open-access article that was selected by an in-house editor and fully peer-reviewed by external reviewers. It is distributed in accordance with the Creative Commons Attribution NonCommercial (CC BY-NC 4.0) license, which permits others to distribute, remix, adapt, build upon this work non-commercially, and license their derivative works on different terms, provided the original work is properly cited and the use is non-commercial. See: <https://creativecommons.org/licenses/by-nc/4.0/>

Country of origin: China

ORCID number: Qing-Yu Gao [0009-0005-8738-2754](https://orcid.org/0009-0005-8738-2754); Li-Jia Wang [0000-0002-8175-7720](https://orcid.org/0000-0002-8175-7720); Chao Ma [0000-0002-2473-387X](https://orcid.org/0000-0002-2473-387X).

S-Editor: Qu XL

L-Editor: A

P-Editor: Lei YY

REFERENCES

- 1 Donati F, Casini C, Cervelli R, Morganti R, Boraschi P. Diffusion-weighted MRI of solid pancreatic lesions: Comparison between reduced field-of-view and large field-of-view sequences. *Eur J Radiol* 2021; **143**: 109936 [RCA] [PMID: 34464906 DOI: 10.1016/j.ejrad.2021.109936] [FullText]
- 2 Hu Y, Hu Q, Liu Z, Huang C, Xia L. Histogram analysis comparison of readout-segmented and single-shot echo-planar imaging for differentiating luminal from non-luminal breast cancer. *Sci Rep* 2024; **14**: 12135 [RCA] [PMID: 38802446 DOI: 10.1038/s41598-024-62514-0] [FullText]
- 3 Peng Y, Li Z, Tang H, Wang Y, Hu X, Shen Y, Hu D. Comparison of reduced field-of-view diffusion-weighted imaging (DWI) and

- conventional DWI techniques in the assessment of rectal carcinoma at 3.0T: Image quality and histological T staging. *J Magn Reson Imaging* 2018; **47**: 967-975 [RCA] [PMID: 28691219 DOI: 10.1002/jmri.25814] [FullText]
- 4 **Ma C**, Li YJ, Pan CS, Wang H, Wang J, Chen SY, Lu JP. High resolution diffusion weighted magnetic resonance imaging of the pancreas using reduced field of view single-shot echo-planar imaging at 3 T. *Magn Reson Imaging* 2014; **32**: 125-131 [RCA] [PMID: 24231348 DOI: 10.1016/j.mri.2013.10.005] [FullText]
- 5 **Le Bihan D**, Poupon C, Amadon A, Lethimonnier F. Artifacts and pitfalls in diffusion MRI. *J Magn Reson Imaging* 2006; **24**: 478-488 [RCA] [PMID: 16897692 DOI: 10.1002/jmri.20683] [FullText]
- 6 **Messina C**, Bignone R, Bruno A, Bruno A, Bruno F, Calandri M, Caruso D, Coppolino P, Robertis R, Gentili F, Grazzini I, Natella R, Scalise P, Barile A, Grassi R, Albano D. Diffusion-Weighted Imaging in Oncology: An Update. *Cancers (Basel)* 2020; **12**: 1493 [RCA] [PMID: 32521645 DOI: 10.3390/cancers12061493] [FullText] [Full Text(PDF)]
- 7 **Koh DM**, Collins DJ. Diffusion-weighted MRI in the body: applications and challenges in oncology. *AJR Am J Roentgenol* 2007; **188**: 1622-1635 [RCA] [PMID: 17515386 DOI: 10.2214/AJR.06.1403] [FullText]
- 8 **QIBA**. MR DWI of the ADC, Clinically Feasible Profile. 2022 [DOI: 10.1148/qiba/20221215] [FullText]
- 9 **Boss MA**, Malyarenko D, Partridge S, Obuchowski N, Shukla-Dave A, Winfield JM, Fuller CD, Miller K, Mishra V, Ohliger M, Wilmes LJ, Attariwala R, Andrews T, deSouza NM, Margolis DJ, Chenevert TL. The QIBA Profile for Diffusion-Weighted MRI: Apparent Diffusion Coefficient as a Quantitative Imaging Biomarker. *Radiology* 2024; **313**: e233055 [RCA] [PMID: 39377680 DOI: 10.1148/radiol.233055] [Full Text]
- 10 **Mürtz P**, Flacke S, Träber F, van den Brink JS, Gieseke J, Schild HH. Abdomen: diffusion-weighted MR imaging with pulse-triggered single-shot sequences. *Radiology* 2002; **224**: 258-264 [RCA] [PMID: 12091693 DOI: 10.1148/radiol.2241011117] [FullText]
- 11 **Byeon J**, Kim JY, Cho AH. Readout-segmented echo-planar imaging in diffusion-weighted MR imaging of acute infarction of the brainstem and posterior fossa: comparison of single-shot echo-planar diffusion-weighted sequences. *Clin Imaging* 2015; **39**: 765-769 [RCA] [PMID: 26119255 DOI: 10.1016/j.clinimag.2015.06.001] [FullText]
- 12 **Bogner W**, Pinker K, Zaric O, Baltzer P, Minarikova L, Porter D, Bago-Horvath Z, Dubsy P, Helbich TH, Trattng S, Gruber S. Bilateral diffusion-weighted MR imaging of breast tumors with submillimeter resolution using readout-segmented echo-planar imaging at 7 T. *Radiology* 2015; **274**: 74-84 [RCA] [PMID: 25341078 DOI: 10.1148/radiol.14132340] [FullText]
- 13 **Ahn HS**, Kim SH, Kim JY, Hong MJ, Lee HS. Accelerating acquisition of readout-segmented echo planar imaging (rs-EPI) with a simultaneous multislice (SMS) technique for diffusion-weighted (DW) breast MRI: Evaluation of image quality factors. *Eur J Radiol* 2024; **170**: 111251 [RCA] [PMID: 38128255 DOI: 10.1016/j.ejrad.2023.111251] [FullText]
- 14 **Klingebl M**, Ullrich T, Quentin M, Bonekamp D, Aissa J, Mally D, Arsov C, Albers P, Antoch G, Schimmöller L. Advanced diffusion weighted imaging of the prostate: Comparison of readout-segmented multi-shot, parallel-transmit and single-shot echo-planar imaging. *Eur J Radiol* 2020; **130**: 109161 [RCA] [PMID: 32650128 DOI: 10.1016/j.ejrad.2020.109161] [FullText]
- 15 **Wu CJ**, Wang Q, Zhang J, Wang XN, Liu XS, Zhang YD, Shi HB. Readout-segmented echo-planar imaging in diffusion-weighted imaging of the kidney: comparison with single-shot echo-planar imaging in image quality. *Abdom Radiol (NY)* 2016; **41**: 100-108 [RCA] [PMID: 26830616 DOI: 10.1007/s00261-015-0615-5] [FullText]
- 16 **Zhang H**, Huang H, Zhang Y, Tu Z, Xiao Z, Chen J, Cao D. Diffusion-Weighted MRI to Assess Sacroiliitis: Improved Image Quality and Diagnostic Performance of Readout-Segmented Echo-Planar Imaging (EPI) Over Conventional Single-Shot EPI. *AJR Am J Roentgenol* 2021; **217**: 450-459 [RCA] [PMID: 32903053 DOI: 10.2214/AJR.20.23953] [FullText]
- 17 **Mannelli L**, Monti S, Corrias G, Fung MM, Nyman C, Golia Pernicka JS, Do RKG. Comparison of Navigator Triggering Reduced Field of View and Large Field of View Diffusion-Weighted Imaging of the Pancreas. *J Comput Assist Tomogr* 2019; **43**: 143-148 [RCA] [PMID: 30119065 DOI: 10.1097/RCT.0000000000000778] [FullText]
- 18 **Banerjee S**, Nishimura DG, Shankaranarayanan A, Saritas EU. Reduced field-of-view DWI with robust fat suppression and unrestricted slice coverage using tilted 2D RF excitation. *Magn Reson Med* 2016; **76**: 1668-1676 [RCA] [PMID: 27654126 DOI: 10.1002/mrm.26405] [FullText]
- 19 **Cai JS**, Chen HY, Chen JY, Lu YF, Sun JZ, Zhou Y, Yu RS. Reduced field-of-view diffusion-weighted imaging (DWI) in patients with gastric cancer: Comparison with conventional DWI techniques at 3.0T: A preliminary study. *Medicine (Baltimore)* 2020; **99**: e18616 [RCA] [PMID: 31895817 DOI: 10.1097/MD.00000000000018616] [FullText] [Full Text(PDF)]
- 20 **Koc Z**, Erbay G. Optimal b value in diffusion-weighted imaging for differentiation of abdominal lesions. *J Magn Reson Imaging* 2014; **40**: 559-566 [RCA] [PMID: 24115207 DOI: 10.1002/jmri.24403] [FullText]
- 21 **Fukukura Y**, Shindo T, Hakamada H, Takumi K, Umanodan T, Nakajo M, Kamimura K, Umanodan A, Ideue J, Yoshiura T. Diffusion-weighted MR imaging of the pancreas: optimizing b-value for visualization of pancreatic adenocarcinoma. *Eur Radiol* 2016; **26**: 3419-3427 [RCA] [PMID: 26738506 DOI: 10.1007/s00330-015-4174-5] [FullText]
- 22 **Ma C**, Liu L, Li YJ, Chen LG, Pan CS, Zhang Y, Wang H, Chen SY, Lu JP. Intravoxel incoherent motion MRI of the healthy pancreas: Monoexponential and biexponential apparent diffusion parameters of the normal head, body and tail. *J Magn Reson Imaging* 2015; **41**: 1236-1241 [RCA] [PMID: 24979657 DOI: 10.1002/jmri.24684] [FullText]
- 23 **Bennett KM**, Schmainda KM, Bennett RT, Rowe DB, Lu H, Hyde JS. Characterization of continuously distributed cortical water diffusion rates with a stretched-exponential model. *Magn Reson Med* 2003; **50**: 727-734 [RCA] [PMID: 14523958 DOI: 10.1002/mrm.10581] [FullText]
- 24 **Li H**, Liang L, Li A, Hu Y, Hu D, Li Z, Kamel IR. Monoexponential, biexponential, and stretched exponential diffusion-weighted imaging models: Quantitative biomarkers for differentiating renal clear cell carcinoma and minimal fat angiomyolipoma. *J Magn Reson Imaging* 2017; **46**: 240-247 [RCA] [PMID: 27859853 DOI: 10.1002/jmri.25524] [FullText]
- 25 **Arab A**, Wojna-Pelczar A, Khairnar A, Szabó N, Ruda-Kucerova J. Principles of diffusion kurtosis imaging and its role in early diagnosis of neurodegenerative disorders. *Brain Res Bull* 2018; **139**: 91-98 [RCA] [PMID: 29378223 DOI: 10.1016/j.brainresbull.2018.01.015] [FullText]
- 26 **Abuzeid HM**, Yassin A, Kamel OF, Sabry KA. Role of diffusion-weighted MR imaging in diagnosis of acute pancreatitis. *Egypt J Radiol Nuc Med* 2020; **51**: 202 [RCA] [DOI: 10.1186/s43055-020-00242-x] [FullText]
- 27 **Wang L**, Gaddam S, Wang N, Xie Y, Deng Z, Zhou Z, Fan Z, Jiang T, Christodoulou AG, Han F, Lo SK, Wachsman AM, Hendifar AE, Pandol SJ, Li D. Multiparametric Mapping Magnetic Resonance Imaging of Pancreatic Disease. *Front Physiol* 2020; **11**: 8 [RCA] [PMID: 32153416 DOI: 10.3389/fphys.2020.00008] [FullText] [Full Text(PDF)]
- 28 **Issa Y**, van Santvoort HC, Fockens P, Besselink MG, Bollen TL, Bruno MJ, Boermeester MA; Collaborators. Diagnosis and treatment in chronic pancreatitis: an international survey and case vignette study. *HPB (Oxford)* 2017; **19**: 978-985 [RCA] [PMID: 28821411 DOI: 10.1016/j.hpb.2017.07.006] [FullText]

- 29 **Zhu M**, Zhang C, Yan J, Sun J, Zhao X, Zhang L, Yin L. Accuracy of quantitative diffusion-weighted imaging for differentiating benign and malignant pancreatic lesions: a systematic review and meta-analysis. *Eur Radiol* 2021; **31**: 7746-7759 [RCA] [PMID: 33847811 DOI: 10.1007/s00330-021-07880-3] [FullText]
- 30 **Nadolska K**, Bialecka A, Zawada E, Kazimierzak W, Serafin Z. Analysis of IVIM Perfusion Fraction Improves Detection of Pancreatic Ductal Adenocarcinoma. *Diagnostics (Basel)* 2024; **14**: 571 [RCA] [PMID: 38534992 DOI: 10.3390/diagnostics14060571] [FullText] [Full Text(PDF)]
- 31 **Kamisawa T**, Takuma K, Anjiki H, Egawa N, Hata T, Kurata M, Honda G, Tsuruta K, Suzuki M, Kamata N, Sasaki T. Differentiation of autoimmune pancreatitis from pancreatic cancer by diffusion-weighted MRI. *Am J Gastroenterol* 2010; **105**: 1870-1875 [RCA] [PMID: 20216538 DOI: 10.1038/ajg.2010.87] [FullText]
- 32 **Hur BY**, Lee JM, Lee JE, Park JY, Kim SJ, Joo I, Shin CI, Baek JH, Kim JH, Han JK, Choi BI. Magnetic resonance imaging findings of the mass-forming type of autoimmune pancreatitis: comparison with pancreatic adenocarcinoma. *J Magn Reson Imaging* 2012; **36**: 188-197 [RCA] [PMID: 22371378 DOI: 10.1002/jmri.23609] [FullText]
- 33 **Muhi A**, Ichikawa T, Motosugi U, Sou H, Sano K, Tsukamoto T, Fatima Z, Araki T. Mass-forming autoimmune pancreatitis and pancreatic carcinoma: differential diagnosis on the basis of computed tomography and magnetic resonance cholangiopancreatography, and diffusion-weighted imaging findings. *J Magn Reson Imaging* 2012; **35**: 827-836 [RCA] [PMID: 22069025 DOI: 10.1002/jmri.22881] [FullText]
- 34 **Choi SY**, Kim SH, Kang TW, Song KD, Park HJ, Choi YH. Differentiating Mass-Forming Autoimmune Pancreatitis From Pancreatic Ductal Adenocarcinoma on the Basis of Contrast-Enhanced MRI and DWI Findings. *AJR Am J Roentgenol* 2016; **206**: 291-300 [RCA] [PMID: 26797355 DOI: 10.2214/AJR.15.14974] [FullText]
- 35 **Jia H**, Li J, Huang W, Lin G. Multimodal magnetic resonance imaging of mass-forming autoimmune pancreatitis: differential diagnosis with pancreatic ductal adenocarcinoma. *BMC Med Imaging* 2021; **21**: 149 [RCA] [PMID: 34654379 DOI: 10.1186/s12880-021-00679-0] [FullText] [Full Text(PDF)]
- 36 **Ha J**, Choi SH, Kim KW, Kim JH, Kim HJ. MRI features for differentiation of autoimmune pancreatitis from pancreatic ductal adenocarcinoma: A systematic review and meta-analysis. *Dig Liver Dis* 2022; **54**: 849-856 [RCA] [PMID: 34903501 DOI: 10.1016/j.dld.2021.11.013] [FullText]
- 37 **De Robertis R**, Cardobi N, Ortolani S, Tinazzi Martini P, Stemmer A, Grimm R, Gobbo S, Butturini G, D'Onofrio M. Intravoxel incoherent motion diffusion-weighted MR imaging of solid pancreatic masses: reliability and usefulness for characterization. *Abdom Radiol (NY)* 2019; **44**: 131-139 [RCA] [PMID: 29951899 DOI: 10.1007/s00261-018-1684-z] [FullText]
- 38 **Zeng P**, Ma L, Liu J, Song Z, Liu J, Yuan H. The diagnostic value of intravoxel incoherent motion diffusion-weighted imaging for distinguishing nonhypervascular pancreatic neuroendocrine tumors from pancreatic ductal adenocarcinomas. *Eur J Radiol* 2022; **150**: 110261 [RCA] [PMID: 35316674 DOI: 10.1016/j.ejrad.2022.110261] [FullText]
- 39 **Bieliuniene E**, Frokjær JB, Pocevičius A, Kemesiene J, Lukosevicius S, Basevicius A, Barauskas G, Dambrauskas Z, Gulbinas A. Magnetic Resonance Imaging as a Valid Noninvasive Tool for the Assessment of Pancreatic Fibrosis. *Pancreas* 2019; **48**: 85-93 [RCA] [PMID: 30451794 DOI: 10.1097/MPA.0000000000001206] [FullText]
- 40 **Wang ZH**, Zhu L, Xue HD, Jin ZY. Quantitative MR imaging biomarkers for distinguishing inflammatory pancreatic mass and pancreatic cancer—a systematic review and meta-analysis. *Eur Radiol* 2024; **34**: 6738-6750 [RCA] [PMID: 38639911 DOI: 10.1007/s00330-024-10720-9] [FullText]
- 41 **Fukukura Y**, Kanki A. Quantitative Magnetic Resonance Imaging for the Pancreas: Current Status. *Invest Radiol* 2024; **59**: 69-77 [RCA] [PMID: 37433065 DOI: 10.1097/RLI.0000000000001002] [FullText]
- 42 **Granata V**, Grassi R, Fusco R, Setola SV, Palaia R, Belli A, Miele V, Brunese L, Grassi R, Petrillo A, Izzo F. Assessment of Ablation Therapy in Pancreatic Cancer: The Radiologist's Challenge. *Front Oncol* 2020; **10**: 560952 [RCA] [PMID: 33330028 DOI: 10.3389/fonc.2020.560952] [FullText] [Full Text(PDF)]
- 43 **Fujita N**, Nishie A, Asayama Y, Ishigami K, Fujimori N, Ito T, Honda H. Intravoxel incoherent motion magnetic resonance imaging for assessment of chronic pancreatitis with special focus on its early stage. *Acta Radiol* 2020; **61**: 579-585 [RCA] [PMID: 31475847 DOI: 10.1177/0284185119872687] [FullText]
- 44 **Liu Q**, Zhang J, Jiang M, Zhang Y, Chen T, Zhang J, Li B, Chen J, Xing W. Evaluating the Histopathology of Pancreatic Ductal Adenocarcinoma by Intravoxel Incoherent Motion-Diffusion Weighted Imaging Comparing With Diffusion-Weighted Imaging. *Front Oncol* 2021; **11**: 670085 [RCA] [PMID: 34249707 DOI: 10.3389/fonc.2021.670085] [FullText] [Full Text(PDF)]
- 45 **Mccullum L**, Jacobson G, Tahon N, Bhosale P, Taniguchi C, Ma J, Tamm E, Koay E, Niedzielski J. Intravoxel Incoherent Motion (IVIM) Magnetic Resonance Imaging (MRI) for Assessment of Treatment Response in Pancreatic Cancer. *Int J Radiat Oncol Biol Phys* 2023; **117**: S65 [RCA] [DOI: 10.1016/j.ijrobp.2023.06.366] [FullText]
- 46 **Shi YJ**, Li XT, Zhang XY, Zhu HT, Liu YL, Wei YY, Sun YS. Non-gaussian models of 3-Tesla diffusion-weighted MRI for the differentiation of pancreatic ductal adenocarcinomas from neuroendocrine tumors and solid pseudopapillary neoplasms. *Magn Reson Imaging* 2021; **83**: 68-76 [RCA] [PMID: 34314825 DOI: 10.1016/j.mri.2021.07.006] [FullText]
- 47 **Li J**, Liang L, Yu H, Shen Y, Hu Y, Hu D, Tang H, Li Z. Whole-tumor histogram analysis of non-Gaussian distribution DWI parameters to differentiation of pancreatic neuroendocrine tumors from pancreatic ductal adenocarcinomas. *Magn Reson Imaging* 2019; **55**: 52-59 [RCA] [PMID: 30240758 DOI: 10.1016/j.mri.2018.09.017] [FullText]
- 48 **Marrale M**, Collura G, Brai M, Toschi N, Midiri F, La Tona G, Lo Casto A, Gagliardo C. Physics, Techniques and Review of Neuroradiological Applications of Diffusion Kurtosis Imaging (DKI). *Clin Neuroradiol* 2016; **26**: 391-403 [RCA] [PMID: 26589207 DOI: 10.1007/s00062-015-0469-9] [FullText]
- 49 **Wu EX**, Cheung MM. MR diffusion kurtosis imaging for neural tissue characterization. *NMR Biomed* 2010; **23**: 836-848 [RCA] [PMID: 20623793 DOI: 10.1002/nbm.1506] [FullText]
- 50 **Fieremans E**, Jensen JH, Helpert JA. White matter characterization with diffusional kurtosis imaging. *Neuroimage* 2011; **58**: 177-188 [RCA] [PMID: 21699989 DOI: 10.1016/j.neuroimage.2011.06.006] [FullText] [Full Text(PDF)]
- 51 **Das CJ**, Malagi AV, Sharma R, Mehndiratta A, Kumar V, Khan MA, Seth A, Kaushal S, Nayak B, Kumar R, Gupta AK. Intravoxel incoherent motion and diffusion kurtosis imaging and their machine-learning-based texture analysis for detection and assessment of prostate cancer severity at 3 T. *NMR Biomed* 2024; **37**: e5144 [RCA] [PMID: 38556777 DOI: 10.1002/nbm.5144] [FullText]
- 52 **Chen PK**, Cheng ZY, Wang YL, Xu BJ, Yu ZC, Li ZX, Gong SA, Zhang FT, Qian L, Cui W, Feng YZ, Cai XR. Renal interstitial fibrotic assessment using non-Gaussian diffusion kurtosis imaging in a rat model of hyperuricemia. *BMC Med Imaging* 2024; **24**: 78 [RCA] [PMID:

- 38570748 DOI: 10.1186/s12880-024-01259-8] [FullText]
- 53 **Zhang Z**, Liu J, Zhang Y, Qu F, Grimm R, Cheng J, Wang W, Zhu J, Li S. T1 mapping as a quantitative imaging biomarker for diagnosing cervical cancer: a comparison with diffusion kurtosis imaging. *BMC Med Imaging* 2024; **24**: 16 [RCA] [PMID: 38200447 DOI: 10.1186/s12880-024-01191-x] [FullText]
- 54 **Granata V**, Fusco R, Sansone M, Grassi R, Maio F, Palaia R, Tatangelo F, Botti G, Grimm R, Curley S, Avallone A, Izzo F, Petrillo A. Magnetic resonance imaging in the assessment of pancreatic cancer with quantitative parameter extraction by means of dynamic contrast-enhanced magnetic resonance imaging, diffusion kurtosis imaging and intravoxel incoherent motion diffusion-weighted imaging. *Therap Adv Gastroenterol* 2020; **13**: 1756284819885052 [RCA] [PMID: 32499833 DOI: 10.1177/1756284819885052] [FullText] [Full Text(PDF)]
- 55 **Mayer P**, Jiang Y, Kuder TA, Bergmann F, Khristenko E, Steinle V, Kaiser J, Hackert T, Kauczor HU, Klauß M, Gaida MM. Diffusion Kurtosis Imaging-A Superior Approach to Assess Tumor-Stroma Ratio in Pancreatic Ductal Adenocarcinoma. *Cancers (Basel)* 2020; **12**: 1656 [RCA] [PMID: 32580519 DOI: 10.3390/cancers12061656] [FullText] [Full Text(PDF)]
- 56 **Granata V**, Fusco R, Setola SV, Palaia R, Albino V, Piccirillo M, Grimm R, Petrillo A, Izzo F. Diffusion kurtosis imaging and conventional diffusion weighted imaging to assess electrochemotherapy response in locally advanced pancreatic cancer. *Radiol Oncol* 2019; **53**: 15-24 [RCA] [PMID: 30681974 DOI: 10.2478/raon-2019-0004] [FullText] [Full Text(PDF)]
- 57 **Zhang Z**, Zhang Y, Hu F, Xie T, Liu W, Xiang H, Li X, Chen L, Zhou Z. Value of diffusion kurtosis MR imaging and conventional diffusion weighed imaging for evaluating response to first-line chemotherapy in unresectable pancreatic cancer. *Cancer Imaging* 2024; **24**: 29 [RCA] [PMID: 38409049 DOI: 10.1186/s40644-024-00674-y] [FullText]
- 58 **Braithwaite AC**, Dale BM, Boll DT, Merkle EM. Short- and midterm reproducibility of apparent diffusion coefficient measurements at 3.0-T diffusion-weighted imaging of the abdomen. *Radiology* 2009; **250**: 459-465 [RCA] [PMID: 19095786 DOI: 10.1148/radiol.2502080849] [Full Text]
- 59 **Corona-Villalobos CP**, Pan L, Halappa VG, Bonekamp S, Lorenz CH, Eng J, Kamel IR. Agreement and reproducibility of apparent diffusion coefficient measurements of dual-b-value and multi-b-value diffusion-weighted magnetic resonance imaging at 1.5 Tesla in phantom and in soft tissues of the abdomen. *J Comput Assist Tomogr* 2013; **37**: 46-51 [RCA] [PMID: 23321832 DOI: 10.1097/RCT.0b013e3182720e07] [Full Text]
- 60 **Chen S**, Liu R, Ma C, Bian Y, Li J, Yang P, Wang M, Lu J. Repeatability of Apparent Diffusion Coefficient at 3.0 Tesla in Normal Pancreas. *Cureus* 2021; **13**: e15734 [RCA] [PMID: 34285845 DOI: 10.7759/cureus.15734] [FullText] [Full Text(PDF)]
- 61 **Barbieri S**, Gurney-Champion OJ, Klaassen R, Thoeny HC. Deep learning how to fit an intravoxel incoherent motion model to diffusion-weighted MRI. *Magn Reson Med* 2020; **83**: 312-321 [RCA] [PMID: 31389081 DOI: 10.1002/mrm.27910] [FullText]
- 62 **Kaandorp MPT**, Barbieri S, Klaassen R, van Laarhoven HWM, Crezee H, While PT, Nederveen AJ, Gurney-Champion OJ. Improved unsupervised physics-informed deep learning for intravoxel incoherent motion modeling and evaluation in pancreatic cancer patients. *Magn Reson Med* 2021; **86**: 2250-2265 [RCA] [PMID: 34105184 DOI: 10.1002/mrm.28852] [FullText] [Full Text(PDF)]
- 63 **Hammernik K**, Klatzer T, Kobler E, Recht MP, Sodickson DK, Pock T, Knoll F. Learning a variational network for reconstruction of accelerated MRI data. *Magn Reson Med* 2018; **79**: 3055-3071 [RCA] [PMID: 29115689 DOI: 10.1002/mrm.26977] [FullText]
- 64 **Aggarwal HK**, Mani MP, Jacob M. MoDL-MUSSELS: Model-Based Deep Learning for Multishot Sensitivity-Encoded Diffusion MRI. *IEEE Trans Med Imaging* 2020; **39**: 1268-1277 [RCA] [PMID: 31603819 DOI: 10.1109/TMI.2019.2946501] [FullText]
- 65 **Troelstra MA**, Van Dijk AM, Witjes JJ, Mak AL, Zwirs D, Runge JH, Verheij J, Beuers UH, Nieuwdorp M, Holleboom AG, Nederveen AJ, Gurney-Champion OJ. Self-supervised neural network improves tri-exponential intravoxel incoherent motion model fitting compared to least-squares fitting in non-alcoholic fatty liver disease. *Front Physiol* 2022; **13**: 942495 [RCA] [PMID: 36148303 DOI: 10.3389/fphys.2022.942495] [FullText] [Full Text(PDF)]
- 66 **Shi YJ**, Zhu HT, Li XT, Zhang XY, Liu YL, Wei YY, Sun YS. Histogram array and convolutional neural network of DWI for differentiating pancreatic ductal adenocarcinomas from solid pseudopapillary neoplasms and neuroendocrine neoplasms. *Clin Imaging* 2023; **96**: 15-22 [RCA] [PMID: 36736182 DOI: 10.1016/j.clinimag.2023.01.008] [FullText]
- 67 **Fokkinga E**, Hernandez-Tamames JA, Ianus A, Nilsson M, Tax CMW, Perez-Lopez R, Grussu F. Advanced Diffusion-Weighted MRI for Cancer Microstructure Assessment in Body Imaging, and Its Relationship With Histology. *J Magn Reson Imaging* 2024; **60**: 1278-1304 [RCA] [PMID: 38032021 DOI: 10.1002/jmri.29144] [FullText]
- 68 **Meyer HJ**, Wienke A, Surov A. ADC values of benign and high grade meningiomas and associations with tumor cellularity and proliferation - A systematic review and meta-analysis. *J Neurol Sci* 2020; **415**: 116975 [RCA] [PMID: 32535250 DOI: 10.1016/j.jns.2020.116975] [FullText]
- 69 **Wang S**, Peng Y, Medved M, Yousuf AN, Ivancevic MK, Karademir I, Jiang Y, Antic T, Sammet S, Oto A, Karczmar GS. Hybrid multidimensional T(02) and diffusion-weighted MRI for prostate cancer detection. *J Magn Reson Imaging* 2014; **39**: 781-788 [RCA] [PMID: 23908146 DOI: 10.1002/jmri.24212] [FullText]
- 70 **Sadinski M**, Karczmar G, Peng Y, Wang S, Jiang Y, Medved M, Yousuf A, Antic T, Oto A. Pilot Study of the Use of Hybrid Multidimensional T2-Weighted Imaging-DWI for the Diagnosis of Prostate Cancer and Evaluation of Gleason Score. *AJR Am J Roentgenol* 2016; **207**: 592-598 [RCA] [PMID: 27352026 DOI: 10.2214/AJR.15.15626] [FullText]
- 71 **Chatterjee A**, Bourne RM, Wang S, Devaraj A, Gallan AJ, Antic T, Karczmar GS, Oto A. Diagnosis of Prostate Cancer with Noninvasive Estimation of Prostate Tissue Composition by Using Hybrid Multidimensional MR Imaging: A Feasibility Study. *Radiology* 2018; **287**: 864-873 [RCA] [PMID: 29393821 DOI: 10.1148/radiol.2018171130] [FullText]
- 72 **Zhang Z**, Wu HH, Priester A, Magyar C, Afshari Mirak S, Shakeri S, Mohammadian Bajgirani A, Hosseiny M, Azadikhah A, Sung K, Reiter RE, Sisk AE, Raman S, Enzmann DR. Prostate Microstructure in Prostate Cancer Using 3-T MRI with Diffusion-Relaxation Correlation Spectrum Imaging: Validation with Whole-Mount Digital Histopathology. *Radiology* 2020; **296**: 348-355 [RCA] [PMID: 32515678 DOI: 10.1148/radiol.2020192330] [FullText]
- 73 **Chatterjee A**, Mercado C, Bourne RM, Yousuf A, Hess B, Antic T, Eggner S, Oto A, Karczmar GS. Validation of Prostate Tissue Composition by Using Hybrid Multidimensional MRI: Correlation with Histologic Findings. *Radiology* 2022; **302**: 368-377 [RCA] [PMID: 34751615 DOI: 10.1148/radiol.2021204459] [FullText]
- 74 **Gibbs P**, Liney GP, Pickles MD, Zehlf B, Rodrigues G, Turnbull LW. Correlation of ADC and T2 measurements with cell density in prostate cancer at 3.0 Tesla. *Invest Radiol* 2009; **44**: 572-576 [RCA] [PMID: 19692841 DOI: 10.1097/RLI.0b013e3181b4c10e] [FullText]
- 75 **Soylu FN**, Peng Y, Jiang Y, Wang S, Schmid-Tannwald C, Sethi I, Eggner S, Antic T, Oto A. Seminal vesicle invasion in prostate cancer: evaluation by using multiparametric endorectal MR imaging. *Radiology* 2013; **267**: 797-806 [RCA] [PMID: 23440325 DOI: 10.1148/radiol.13121319] [FullText]

- 76 **Wu LM**, Xu JR, Ye YQ, Lu Q, Hu JN. The clinical value of diffusion-weighted imaging in combination with T2-weighted imaging in diagnosing prostate carcinoma: a systematic review and meta-analysis. *AJR Am J Roentgenol* 2012; **199**: 103-110 [RCA] [PMID: 22733900 DOI: 10.2214/AJR.11.7634] [FullText]
- 77 **Kim D**, Doyle EK, Wisnowski JL, Kim JH, Haldar JP. Diffusion-relaxation correlation spectroscopic imaging: A multidimensional approach for probing microstructure. *Magn Reson Med* 2017; **78**: 2236-2249 [RCA] [PMID: 28317261 DOI: 10.1002/mrm.26629] [FullText]
- 78 **Liu F**, Hu W, Sun Y, Shen Y, Zhou W, Dai Y, Gu L, Zhang M, Zhou Y. Exploration of Interstitial Fibrosis in Chronic Kidney Disease by Diffusion-Relaxation Correlation Spectrum MR Imaging: A Preliminary Study. *J Magn Reson Imaging* 2023; **58**: 415-426 [RCA] [PMID: 36412255 DOI: 10.1002/jmri.28535] [FullText]
- 79 **Luo Y**, Zhu M, Wei X, Xu J, Pan S, Liu G, Song Y, Hu W, Dai Y, Wu G. Investigation of clear cell renal cell carcinoma grades using diffusion-relaxation correlation spectroscopic imaging with optimized spatial-spectrum analysis. *Br J Radiol* 2024; **97**: 135-141 [RCA] [PMID: 38263829 DOI: 10.1093/bjr/tqad003] [FullText]
- 80 **Hua W**, Xiao T, Jiang X, Liu Z, Wang M, Zheng H, Wang S. Lymph-vascular space invasion prediction in cervical cancer: Exploring radiomics and deep learning multilevel features of tumor and peritumor tissue on multiparametric MRI. *Biomed Signal Process Control* 2020; **58**: 101869 [RCA] [DOI: 10.1016/j.bspc.2020.101869] [FullText]
- 81 **Su CQ**, Wang BB, Tang WT, Tao C, Zhao P, Pan MH, Hong XN, Hu WT, Dai YM, Shi HB, Lu SS. Diffusion-relaxation correlation spectrum imaging for predicting tumor consistency and gross total resection in patients with pituitary adenomas: a preliminary study. *Eur Radiol* 2023; **33**: 6993-7002 [RCA] [PMID: 37148353 DOI: 10.1007/s00330-023-09694-x] [FullText]
- 82 **Chen W**, Geng D, Xu XQ, Hu WT, Dai YM, Wu FY, Zhu LN. Characterization of parotid gland tumors using diffusion-relaxation correlation spectrum imaging: a preliminary study. *Clin Radiol* 2024; **79**: e878-e884 [RCA] [PMID: 38582630 DOI: 10.1016/j.crad.2024.02.006] [FullText]
- 83 **Edelman RR**, Salanitri G, Brand R, Dunkle E, Ragin A, Li W, Mehta U, Berlin J, Newmark G, Gore R, Patel B, Carillo A, Vu A. Magnetic resonance imaging of the pancreas at 3.0 tesla: qualitative and quantitative comparison with 1.5 tesla. *Invest Radiol* 2006; **41**: 175-180 [RCA] [PMID: 16428989 DOI: 10.1097/01.rli.0000195880.69880.6c] [FullText]
- 84 **Kim JH**, Byun JH, Kim MH, Lee SK, Kim SC, Kim HJ, Lee SS, Kim SY, Lee MG. Pancreatic Duct in Autoimmune Pancreatitis: Intraindividual Comparison of Magnetic Resonance Pancreatography at 1.5 T and 3.0 T. *Pancreas* 2017; **46**: 921-926 [RCA] [PMID: 28697133 DOI: 10.1097/MPA.0000000000000853] [FullText]
- 85 **Harrington KA**, Shukla-Dave A, Paudyal R, Do RKG. MRI of the Pancreas. *J Magn Reson Imaging* 2021; **53**: 347-359 [RCA] [PMID: 32302044 DOI: 10.1002/jmri.27148] [FullText]
- 86 **Barral M**, Taouli B, Guiu B, Koh DM, Luciani A, Manfredi R, Vilgrain V, Hoeffel C, Kanematsu M, Soyer P. Diffusion-weighted MR imaging of the pancreas: current status and recommendations. *Radiology* 2015; **274**: 45-63 [RCA] [PMID: 25531479 DOI: 10.1148/radiol.14130778] [FullText]
- 87 **Xu F**, Liang Y, Guo W, Liang Z, Li L, Xiong Y, Ye G, Zeng X. Diagnostic Performance of Diffusion-Weighted Imaging for Differentiating Malignant From Benign Intraductal Papillary Mucinous Neoplasms of the Pancreas: A Systematic Review and Meta-Analysis. *Front Oncol* 2021; **11**: 637681 [RCA] [PMID: 34290974 DOI: 10.3389/fonc.2021.637681] [FullText] [Full Text(PDF)]
- 88 **Taouli B**, Beer AJ, Chenevert T, Collins D, Lehman C, Matos C, Padhani AR, Rosenkrantz AB, Shukla-Dave A, Sigmund E, Tanenbaum L, Thoeny H, Thomassin-Naggara I, Barbieri S, Corcuera-Solano I, Orton M, Partridge SC, Koh DM. Diffusion-weighted imaging outside the brain: Consensus statement from an ISMRM-sponsored workshop. *J Magn Reson Imaging* 2016; **44**: 521-540 [RCA] [PMID: 26892827 DOI: 10.1002/jmri.25196] [FullText]
- 89 **Rosenkrantz AB**, Oei M, Babb JS, Niver BE, Taouli B. Diffusion-weighted imaging of the abdomen at 3.0 Tesla: image quality and apparent diffusion coefficient reproducibility compared with 1.5 Tesla. *J Magn Reson Imaging* 2011; **33**: 128-135 [RCA] [PMID: 21182130 DOI: 10.1002/jmri.22395] [FullText]
- 90 **Zheng L**, Yang C, Liang L, Rao S, Dai Y, Zeng M. T2-weighted MRI and reduced-FOV diffusion-weighted imaging of the human pancreas at 5 T: A comparison study with 3 T. *Med Phys* 2023; **50**: 344-353 [RCA] [PMID: 36107133 DOI: 10.1002/mp.15970] [FullText]
- 91 **Zhang Y**, Sheng R, Yang C, Dai Y, Zeng M. Higher field reduced FOV diffusion-weighted imaging for abdominal imaging at 5.0 Tesla: image quality evaluation compared with 3.0 Tesla. *Insights Imaging* 2023; **14**: 171 [RCA] [PMID: 37840062 DOI: 10.1186/s13244-023-01513-7] [FullText]
- 92 **Jiang Z**, Sun W, Xu D, Yu H, Mei H, Song X, Xu H. Stability and repeatability of diffusion-weighted imaging (DWI) of normal pancreas on 5.0 Tesla magnetic resonance imaging (MRI). *Sci Rep* 2023; **13**: 11954 [RCA] [PMID: 37488151 DOI: 10.1038/s41598-023-38360-x] [FullText] [Full Text(PDF)]
- 93 **Cheng K**, Duan Q, Hu J, Li C, Ma X, Bian X, Duan C, Xiong Y, Lin J, Lu H, Deng L, Li Z, Wei M, Lyu J, Chen L, Lou X. Evaluation of postcontrast images of intracranial tumors at 7T and 3T MRI: An intra-individual comparison study. *CNS Neurosci Ther* 2023; **29**: 559-565 [RCA] [PMID: 36468424 DOI: 10.1111/cns.14036] [FullText]
- 94 **Yao J**, Morrison MA, Jakary A, Avadiappan S, Rowley P, Glueck J, Driscoll T, Geschwind MD, Nelson AB, Possin KL, Xu D, Hess CP, Lupo JM. Altered Iron and Microstructure in Huntington's Disease Subcortical Nuclei: Insight From 7T MRI. *J Magn Reson Imaging* 2024; **60**: 1484-1499 [RCA] [PMID: 38206986 DOI: 10.1002/jmri.29195] [FullText]
- 95 **Alushaj E**, Handfield-Jones N, Kuurstra A, Morava A, Menon RS, Owen AM, Sharma M, Khan AR, MacDonald PA. Increased iron in the substantia nigra pars compacta identifies patients with early Parkinson's disease: A 3T and 7T MRI study. *Neuroimage Clin* 2024; **41**: 103577 [RCA] [PMID: 38377722 DOI: 10.1016/j.nicl.2024.103577] [FullText] [Full Text(PDF)]
- 96 **Heiss R**, Weber MA, Balbach E, Schmitt R, Rehnitz C, Laqmani A, Sternberg A, Ellermann JJ, Nagel AM, Ladd ME, Englbrecht M, Arkudas A, Horch R, Guermazi A, Uder M, Roemer FW. Clinical Application of Ultrahigh-Field-Strength Wrist MRI: A Multireader 3-T and 7-T Comparison Study. *Radiology* 2023; **307**: e220753 [RCA] [PMID: 36625744 DOI: 10.1148/radiol.220753] [FullText]
- 97 **Fujiwara S**, Mori Y, de la Mora DM, Akamatsu Y, Yoshida K, Shibata Y, Masuda T, Ogasawara K, Yoshioka Y. Feasibility of IVIM parameters from diffusion-weighted imaging at 11.7T MRI for detecting ischemic changes in common carotid artery occlusion rats. *Sci Rep* 2020; **10**: 8404 [RCA] [PMID: 32439877 DOI: 10.1038/s41598-020-65310-8] [FullText] [Full Text(PDF)]
- 98 **Zhang T**, Lu Y, Yang B, Zhang C, Li J, Liu H, Wang H, Wang D. Diffusion Metrics for Staging Pancreatic Fibrosis and Correlating With Epithelial-Mesenchymal Transition Markers in a Chronic Pancreatitis Rat Model at 11.7T MRI. *J Magn Reson Imaging* 2020; **52**: 197-206 [RCA] [PMID: 31755193 DOI: 10.1002/jmri.26995] [FullText]



Published by **Baishideng Publishing Group Inc**
7041 Koll Center Parkway, Suite 160, Pleasanton, CA 94566, USA
Telephone: +1-925-3991568
E-mail: office@baishideng.com
Help Desk: <https://www.f6publishing.com/helpdesk>
<https://www.wjgnet.com>

